DYNAMIC STIFFNESS CHARACTERISTICS OF HIGH ECCENTRICITY

RATIO BEARINGS AND SEALS BY PERTURBATION TESTING

Donald E. Bently and Agnes Muszynska
Bently Nevada Corporation
Minden, Nevada 89423

In prior work perturbation methodology was done to describe the behavior of lightly loaded bearings or seals. This work helped to clarify the stiffness algorithms and to show the algorithm of the fluid inertia effect.

This paper takes up the much more complex behavior of cylindrical bearings and seals that are statically loaded to eccentricities in excess of 0.7. The stiffness algorithms as a function of static load are developed from perturbation methodology by empirical modeling.

INTRODUCTION

In prior papers by the authors [1-3] perturbation methodology was employed to study the behavior of lightly loaded seals and bearings.

Most studies of rotor instability mechanisms caused by fluid (liquid, steam, or gas) forces, and studies of the behavior of squeeze film dampers have been to measure, by theory and/or by experiment, the bearing/seal dynamic stiffness characteristics. To this effect, most often the perturbation technique, either by imbalance at rotative speed or by static loading with the rotor at its operational speed has been applied. Such examination is perfectly valid, however, the data of the direct and cross stiffness terms are limited to those two data points, instead of across a wide range of perturbation speeds. Because of this, much needed data is not known.

Examination of the direct and quadrature dynamic stiffness characteristics of a rotor system when it is at its operating speed and conditions, is best accomplished by sinusoidal perturbation across the range of speeds where the dynamic stiffness terms are desired. Generally, these are in the range of (a) the average fluid precession rate (usually 40 to 50% of rotative speed in an uncontrolled seal or

bearing), or (b) in the region of the self balance resonances (usually the first one, and usually below operating speed).

In some studies of rotor systems, such as identifying a resonance above maximum operating speed, the perturbation method is easily employed to excite the rotor to obtain this data that is otherwise very difficult or uncertain, or available only from calculation.

For another example, the study of the frequency shift of the forward and reverse resonances due to gyroscopic effects of rotors as a function of rotative speed, the perturbation methodology produces excellent results. For such a study, the rotor is perturbed by circular perturbation, both forward (in direction of shaft rotation), and in reverse (in opposite direction of shaft rotation) for each rotative speed of the rotor system of interest.
Perturbation methodology is also of great assistance in the many faceted studies of full and partial rub mechanisms of a rotor system.

NOTATION

K_D	Direct dynamic stiffness (if symmetric)	lbs/inch
K_{DX}	Direct dynamic stiffness (X axis)	lbs/inch
K_{DY}	Direct dynamic stiffness (Y axis)	lbs/inch
K_Q	Quadrature dynamic stiffness (if symmetric)	lbs/inch
K_{QX}	Quadrature dynamic stiffness (X axis)	lbs/inch
K_{QY}	Quadrature dynamic stiffness (Y axis)	lbs/inch
$K_{ext\ x}$	External spring coefficient (X axis)	lbs/inch
$K_{ext\ y}$	External spring coefficient (Y axis)	lbs/inch
D	Bearing Damping coefficient (if symmetric)	lb sec/inch
D_X	Bearing Damping coefficient (X axis)	lb sec/inch
D_Y	Bearing Damping coefficient (Y axis)	lb sec/inch
M	Rotor effective mass	lb sec^2/inch
M_F	Bearing fluid inertia coefficient (if symmetric)	lb sec^2/inch
M_{FX}	Bearing fluid inertia coefficient (X axis)	lb sec^2/inch
M_{FY}	Bearing fluid inertia coefficient (Y axis)	lb sec^2/inch
ω_R	Rotor rotative speed	rad/sec
ω_P	Perturbation speed (+fwd, -rev)	rad/sec

λ	Ratio of average fluid swirling velocity divided by rotative speed	-----
η	Oil viscosity	centipoise
W_U	Perturbation imbalance	grams
M_U	Perturbation imbalance mass	lb sec^2/inch
R_U	Perturbation imbalance radius	inches
P	Static load on rotor	lbs
A	Angle of application of the static load P measured in direction of shaft rotation from vertical	degrees
$\bar{F}_x$	Force vector in X direction	lbs
$\bar{F}_y$	Force vector in y direction	lbs
t	Time	seconds
j	$\sqrt{-1}$	-----

HISTORY

For several years the authors believed that Ed Hull [4-6] did the first published (and some unpublished) experiments, of perturbing a rotor system across a frequency range (at other than synchronous or steady state) in 1955, but recently found a reference in Paul Trumpler's book [7], to Stone and Underwood [8], dating the methodology back to 1947, so it is possible that other earlier work exists.

Even though these researchers showed the resultant amplitude and phase of the perturbation correctly, neither took the next step of dividing the input force vectors by the motion vectors to obtain the direct and quadrature dynamic stiffnesses. However, both researchers did brilliant work in obtaining vector motion measurements considering the extremely crude electronics tools that were available to them at the time they did their work.

APPLICATION OF PERTURBATION METHODS IN ROTATING MACHINERY

To input a perturbation of either motion or force to a mechanical system, a wide variety of methods may be employed, such as impulse, step white noise, square waves and so forth.

However, when the direct and quadrature dynamic stiffness coefficients of a rotating machine are desired, then the perturbation forcing method becomes highly restricted. It is necessary to use continuous sinusoidal perturbation with high accuracy of phase and amplitude of both the force (perturbation by force) as well as the motion (perturbation by motion).

There is a free choice of driving the system with either a known motion vector and observing the resultant force vectors, or driving the system with a known force vector and observing the motion. However, it is extremely difficult to build a test system to drive a known input motion, and relatively easy to build a system with a known input perturbation force. Further it is much easier to measure response motion vectors than to measure response force vectors. As a result, the authors chose to input with a known amplitude and phase a sinusoidal perturbation force, and observe the response motion vectors. This methodology may be used to test a real rotor system as well as a laboratory experiment. The reduction of the data is equally difficult with either method.

There also appears to be a free choice of whether to apply the perturbation force to the rotor casing or directly on to the shaft. The authors chose to directly perturb the shaft as close as possible to the bearing or seal under test in order to eliminate or minimize the possible errors introduced by the complexities of any other method.

Since two degrees of freedom of the rotor motion are involved, there is one more vital consideration of the sinusoidal perturbation forcing input: (1) it may be in one radial axis, such as vertical (2) it may be circular forward, or circular reverse, or (3) it may be somewhere between these, specifically an ellipse with forward or reverse characteristics.

When gyroscopic effects are the subject of study, it is obvious that circular perturbation force must be employed, as any other force (elliptical or unidirectional), contains a mixture of forward and reverse components. Only forward circular perturbation yields the forward resonances clearly, and only reverse circular perturbation yields the backwards resonances clearly.

The ideal perturbation system when the dynamic stiffnesses are not symmetric is to maintain a resultant perturbation motion of circular nature. This may

be achieved using Adams' method [9] which is to introduce a circular perturbation motion or else to adjust the amplitude and phase of the input perturbation force to obtain a circular motion response. Both methods yield directly reducible dynamic stiffness terms, but both are very difficult to accomplish. As a result, the studies in this report were done with circular sinusoidal foward and reverse input perturbation force, as in previous studies [3].

LABORATORY STUDY OF STABILITY CHARACTERISTICS OF A 360° LUBRICATED CYLINDRICAL BEARING AS A FUNCTION OF STATIC LOAD, ROTATIVE SPEED, OIL SUPPLY PRESSURE, AND VISCOSITY

The experimental rotor set-up for the bearing/seal perturbation test is shown in Figures 1 and 2.

In previous experiments, the authors studied the direct and quadrature stiffness terms of the same bearing and same rotor configuration for light preloads. In the present study, the constant preload was varied from 0 to 32 lbs., (increasing by 4 lbs at each sequence of tests) in order to observe the behavior of the dynamic stiffness terms when the oil film is broken (or partially broken) in the negative pressure region of the bearing. Rotative speeds of 0, 100, 200, 300, 400, 500 and 600 rad/sec were employed with circular perturbation frequencies from - (reverse) 400 rad/sec to + (forward) 400 rad/sec. The bulk of these studies were with a constant perturbation imbalance weight of 28 grams, and with a constant oil supply pressure of 5 psi. At the end of the tests, the oil pressure was raised to 20 psi, with results shown in Figure 5. Temperature was held a oil outlet constant at 65°, 90°F, and 130°F. T-10 turbine oil was employed for all data.

For zero, or light loads and symmetric rotor, the vertical and horizontal force algorithms are:

Eq. (1) $\bar{F}y=[K_{ext}+j\omega_p D-(\lambda\omega_R-\omega_p)^2 M_F]\bar{y} +j[\lambda\omega_R D]\bar{x}$

Eq. (2) $\bar{F}_X=[K_{ext}+j\omega_p D(-\lambda\omega_R-\omega_R)^2]\bar{x}-j[\lambda\omega_R D]\bar{y}$ and since

Eq. (3) $\bar{x}=j\bar{y}$ because the resultant orbit are circular, equations 1 and 2 reduce to:

485

Eq. (4) $\quad \bar{F}_Y = \bar{y}[K_{ext} - (\lambda\omega_R - \omega_p)^2 M_F - \omega_p^2 M + j(\omega_p D - \lambda\omega_R D)]$

Eq. (5) $\quad \bar{F}_X = \bar{x}[K_{ext} - (\lambda\omega_R - \omega_p)^2 M_F - \omega_p^2 M + j(\omega_p D - \lambda\omega_R D)]$

The dynamic stiffness vectors are:

Eq. (6) $\quad \bar{K}_Y = K_D + jK_Q = \bar{F}_y/\bar{y}$

Eq. (7) $\quad \bar{K}_X = K_D + jK_Q = \bar{F}_x/\bar{x}$
$\quad$ with the result that for a symmetrical, lightly loaded 360°
$\quad$ lubricated bearing, or a lightly loaded seal it becomes:

Eq. (8) $\quad K_D = K_{ext} - \omega_p^2 M - (\lambda\omega_R - \omega_p)^2 M_F \qquad$ Direct Dynamic Stiffness

Eq. (9) $\quad K_Q = (\omega_p - \lambda\omega_R)D \qquad\qquad\qquad$ Quadrature Dynamic Stiffness

More detailed deviation of the above relationships can be found in the publications [1-3].

It may be noted that direct dynamic stiffness versus perturbation speed is parabola and offset from zero speed toward the average swirl speed of the oil ($\lambda\omega_R$), and that the quadrature term consists of a straight line with a value of zero at a perturbation speed of exactly $\omega_p = \lambda\omega_R$ (the traditional "½ speed" of oil whirl). The quadrature term at zero frequency perturbation represents the famous tangential term, otherwise known as "aerodynamic cross coupling" term, "cross coupled" spring coefficients "K_{XY}", "K_{YX}", etc. As a matter of fact, this is the oil wedge support term of a cylindrical bearing, from the single action that the shaft must move sideways (at quadrature) a sufficient distance to create a constriction of the oil in order to form a pressure wedge 90° behind this constriction in order to support the load. (As such, a cylindrical bearing or seal is an elementary servomechanism with very poor stability control.)

Static Load Study

Before running the forward and reverse perturbation tests, a complete series of static loading tests were run across the variations of static load, static load

angle, viscosity, and oil pressure while maintaining the rotor constant operational speed. A brief matrix summary of the results of the steady state deflection versus load tests are shown in Figures 3, 4 and 5.

Since ω_p is zero and K_{ext} is also zero for these sets of tests, equations (8) and (9) reduce to the following equations (10) and (11) for the lightly loaded condition. This extends from zero load to wherever the knee (an evident non-linearity) of the static displacement occurs.

(10) $K_D = -\lambda^2 \omega_R^2 M_F$ Static Direct Stiffness

(12) $K_Q = -\lambda \omega_R D$ Static Quadrature Stiffness

Clearly, the fluidic inertia term, $(-\lambda^2 \omega_R^2 M_F)$, controls the direct dynamic stiffness, and equally clearly, the "cross spring" term, (fluid wedge support term $-\lambda \omega_R D$), controls the quadrature stiffness in the lightly loaded bearings.

Since the wedge support term is formed by the shaft moving sideways to the static load to form a restriction to form the wedge support, the shaft deflection is ahead of the static load angle by 90 degrees in the direction of rotation. When the direct term Eq. (8) is net negative, as in the above situation of the negative direct spring effect of fluid inertia, then the shaft attitude angle is in excess of 90 degrees.

Figure 3 shows the curves of attitude angle and eccentricity ratio for various preload at temperatures 65°F, 90°F, and 130°F of T-10 oil. It may be observed that the attitude angle is highest for highest viscosity at light loads, but that this reverses at high static preload. This infers that fluid inertia is a function of viscosity, but it is the belief of the authors that this relationship is a secondary result of the continuity of the oil film in the negative pressure region. This graph (and other results shown later) indicate that if the fluid film in the negative pressure region collapses, or partially collapses, the fluid inertia term is drastically reduced. It is predominantly this effect that is shown in the graph. The variation of the eccentricity ratio and attitude angle as a function of rotative speed at constant oil temperature (90°F) and pressure (5 psi) is shown in Figure 4.

Somewhat similar to the previous picture, the effect reverses from low to high

static load, with ever increasing attitude angle as a function of rotative speed until the knee of the curve (following the fluid inertia term $-\lambda^2 \omega_R^2 M_F$), then reversing at the knee. Again, the authors believe that this loss of the fluid inertia term is primarily a function of the partial collapse of the film in the negative pressure region. Simply, when air moves in, to replace the oil in either the steady state or dynamic negative pressure region, there is no need to jet oil through the thin film region from the high pressure region to the low pressure region; therefore major decrease of the fluidic inertia term occurs.

Figure 5 shows the effect of the static deflection versus static load for oil supply pressure variations from 5 to 25 psi, at constant speed of 200 rad/sec and oil temperature of 90°F. Here a new type of inversion is observed.

Before the knee of the curve, the attitude angle increases with pressure from 5 to 20 psi, but at 25 psi it is clearly reversed. This shows a collapse of the fluid inertia term between 20 and 25 psi supply pressure. It is believed that the collapse of the fluid inertia term in this instance is because the new oil feed to the bearing supplies the negative pressure region, alleviating the need for the fluid inertia effect. Note that this is for a different reason than occurs in the other tests. It should be noted that these deflections versus load graphs also reverse beyond the knee of the curve.

The Perturbation Tests

Hundreds of runs were made to establish the direct and quadrature dynamic stiffness terms. These tests were predominantly run at 5 psi oil supply pressure (with a few at higher pressure), with rotative speeds from 100 rad/sec to 600 rad/sec, in steps of 100 rads/sec, with oil temperatures of 65, 90 and 130°F, (thus viscosities of 64.3, 35.6 and 15 centipoise), with perturbation speeds of 30 to 400 rad/sec, mostly forward, (and enough in reverse to show the typical stiffness behavior), and with a 28 gram perturbation weight at 1.1 inch radius. A very brief summary of these tests are shown in this report.

Figure 6 shows the direct and quadrature dynamic stiffness is at zero and light preloads at three viscosities, at 100 rad/sec, at 5 psi oil supply pressure, and for forward and reverse perturbation. The quadrature stiffness shows its regular performance. (1) zero crossover at 48% of rotative speed, which is the average

swirl ratio λ, (2) a slope, which is D lbs.sec/in of damping directly dependent on viscosity, and (3) the oil wedge support term (cross spring) a direct function of λ, ω_R rotative speed, and D damping.

The direct term shows its typical parabola behavior due primarily to the fluid inertia term. For very light dynamic perturbation loads, as previously studied, the fluid inertia term is independent of viscosity. However, with the heavy dynamic load employed for this test, and for the very low oil supply pressure, the fluid inertia term increases with increasing viscosity. The authors believe that this shift of the fluid inertia term is due to partial loss of the negative pressure region at the lower viscosities.

The figures 7 through 10 show the effects on the dynamic stiffness terms with static loading of 0 to 24 pounds in steps of 4 lbs. These runs are at an oil supply pressure of 5 psi, at an outlet oil temperature of 65°F (64.3 centipoise) and at constant rotative speed of 300 rad/sec.

It may be observed that the dynamic quadrature stiffness tends to increase in slope with higher static load, but that this is a small effect, with a 24 pound static load indicating an increase in damping of about 50 percent over the damping at zero static load.

However, the direct dynamic stiffness show much greater variations with static load, especially (1) at 24 pounds, where a large increase in the dynamic direct vertical spring term occurs, and (2) at perturbation rates from about -10% of rotative speed to about +30% of rotative speed. The horizontal direct dynamic stiffness term shows increase as a function of static loading more evenly for each increment of static load. These results should be related to the deflection versus static load shown in Figures 3 and 4.

CONCLUSIONS

First, it may be concluded that for a 360 degree lubricated bearing a simple algorithm to describe its dynamic behavior is virtually impossible when any condition exists which allows air to be pulled into the negative pressure region. This may be caused by many factors, including low oil supply pressure or broken flow, high static loading, high dynamic loading, low rotative speed, etc. It

follows that it is very difficult to establish a clear mathematic rule for stability for such a bearing. Cole and Hughes [10] stated essentially the same thing on their remarks of a Boeker and Sternlicht paper [11] 30 years ago with less evidence, and apparently no knowledge of the fluid inertia term or extreme possible variations of that term. "During the course of some film extent experiments on a transparent sleeve bearing (1 X 1 X 0.002 in.) with a single-hole oil entry, we have observed that whirl at frequency near to half shaft speed may occur over a wide speed range but only while the film remains complete. As soon as the film breaks, as a result of increased eccentricity ratio or changed oil-supply conditions, whirl ceases."

Second, it is concluded that a 360 degree lubricated bearing is not a good prototype model for work with liquid or gas seals. For liquid seals, the pressure of the supply is orders of magnitude higher than that of typical oil supply pressures, so that the fluid inertia term will be much greater and much more consistent in the speeds of interest. For the gas seal, there can be no occurrence of an incomplete or cavitated film in the negative pressure region, so that much higher similarity may be expected. However, the principle of feeding the test bearing from the center should be a very good method of studying seals, as a seal test rig may be center fed at high pressure, and the low pressure at the ends, which can be equivalent to two halves of a seal with high pressure at one end, and low pressure at the other end. With this configuration a test stand for seals is simple to construct and use, as there is no secondary high pressure seal area on the rotor system. If anti-swirling methods are being employed and tested. However, they would be in opposite directions on opposite ends of the test seal.

REFERENCES:

1. Bently, D.E., Muszynska, A., "Stability Evaluation of Rotor/Bearing System by Perturbation Tests," Rotordynamic Instability Problems in High Performance, Turbomachinery, NASA CP-2250, 1982, pp. 307-322.

2. Bently, D.E., Muszynska, A., "Oil Whirl Identification by Perturbation Test," Advances in Computer-Aided Bearing Design, ASME/ASLE Lubrication Conference, Washington, D.C., October 1982.

3. Bently, D.E., Muszynska, A., "Perturbation Tests of Bearing/Seal For Evaluation of Dynamic Coefficients," Symposium on Rotor Dynamical Instability, Summer Annual Conference of the ASME Applied Mechanics Division, Houston, Texas, June 1983.

4. Hull, E.H., "Journal Bearing Behavior Under Periodic Loading," G.I. Research Laboratory, Rep. No. 55-RL-1354, Schenectady, New York 1955.

5. Hull, E.H., "Oil Whip Resonance," Trans. ASME, October 1958

6. Hull, E.H., Darrow, K.A., "Hydrodynamic Oil Film Stiffness", G.I. Research Laboratory, Rep. No. 59-RL-2217, Schenectady, New York 1959.

7. Trumpler, Paul R., "Design of Film Bearings," Dept. of Mechanical Engineering, University of Pennsylvania, 1966.

8. Stone, J.M., Underwood, F.A., "Load Carrying Capacity of Journal Bearings," SAE Quart. Trans., 1 (1947), p. 56.

9. Adams, A.L., "Rotor Perturbation Test by Forced Motion," Private Communication.

10. Cole, J.A., and Hughes, C.J., "Visual Study of Film Extent in Dynamically Loaded Complete Journal Bearings," Conference on Lubrication and Wear, London, England, 1 October 1957.

11. Boeker, G.F., and Sternlicht,B., "Investigation of Translatory Fluid Whirl in Vertical Machines," ASME/ASLE Lubrication Conference, Baltimore, Marlyland, 18 October 1954.
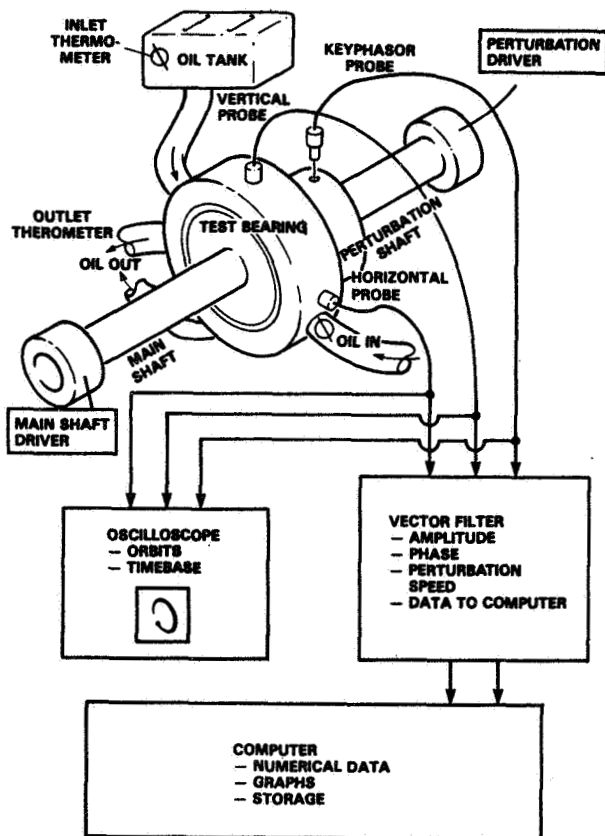
Figure 1. - Experiment setup.
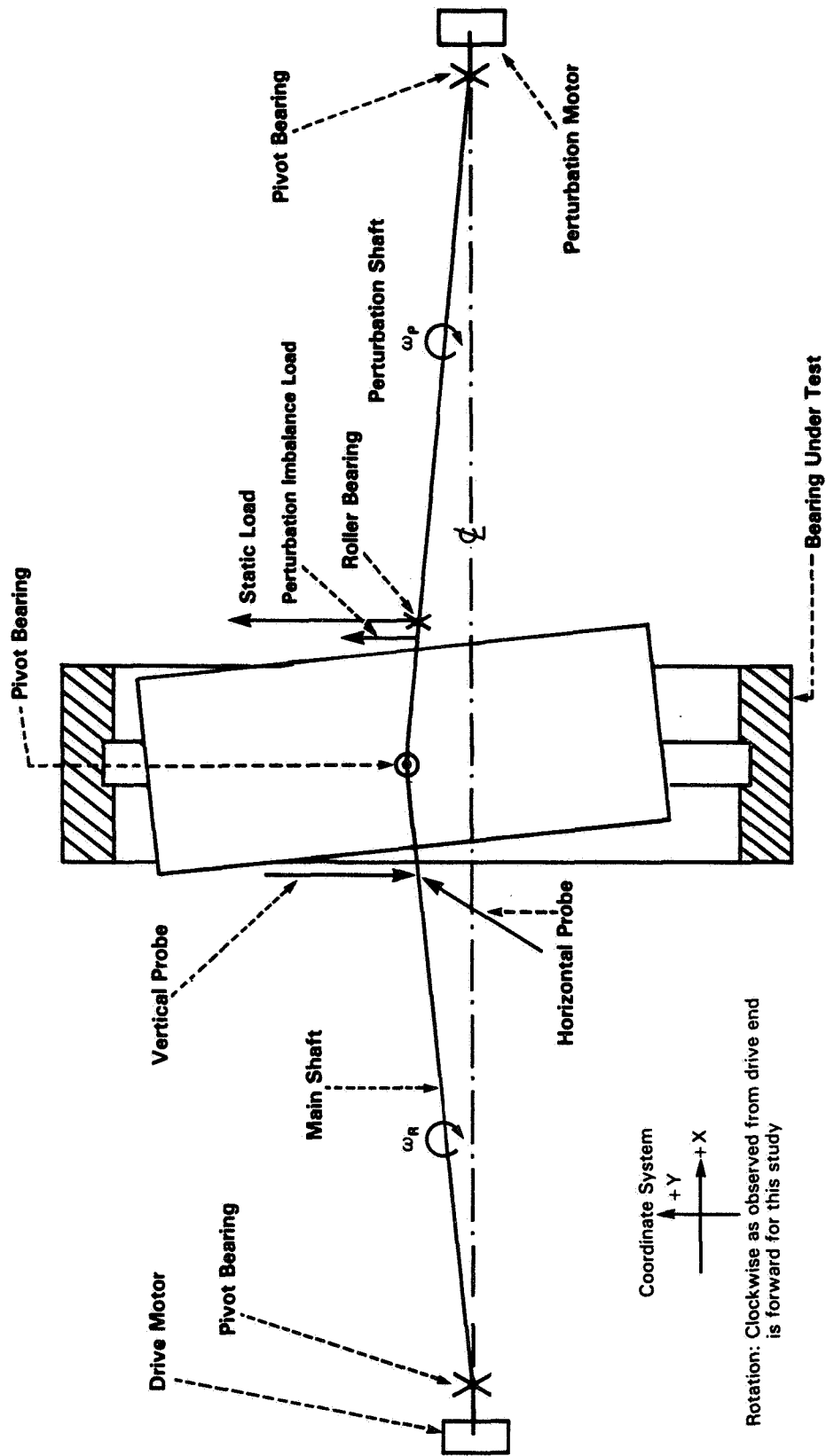
Figure 2. - Diagram of perturbation test system.
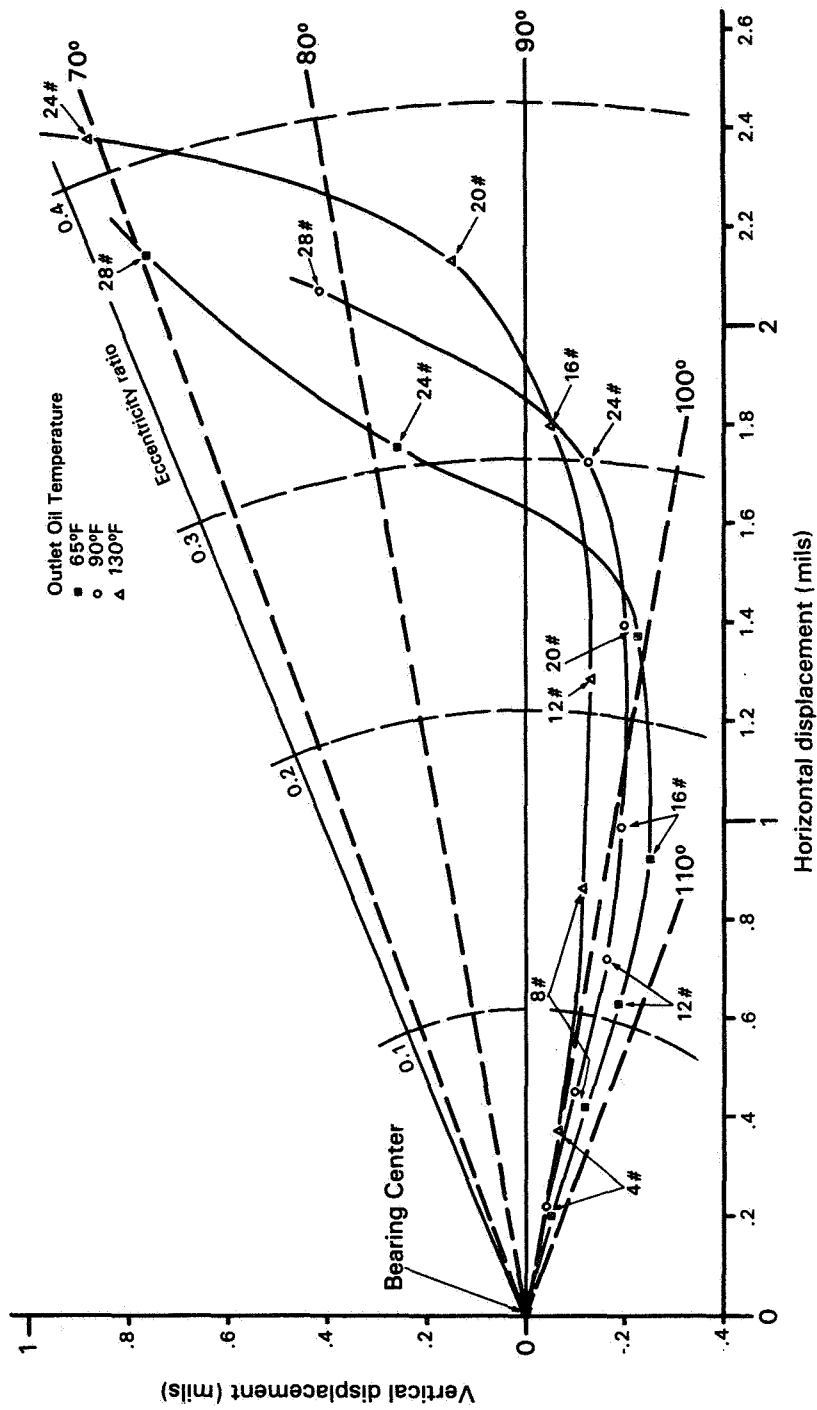
Figure 3. — Static deflection at oil outlet temperatures of 65°, 90°, and 130° F (64.3, 35.6, and 15.7 cP), rotative speed of 400 rad/sec, oil supply pressure of 5 psi, and static loads to 28 lb with clockwise rotation.
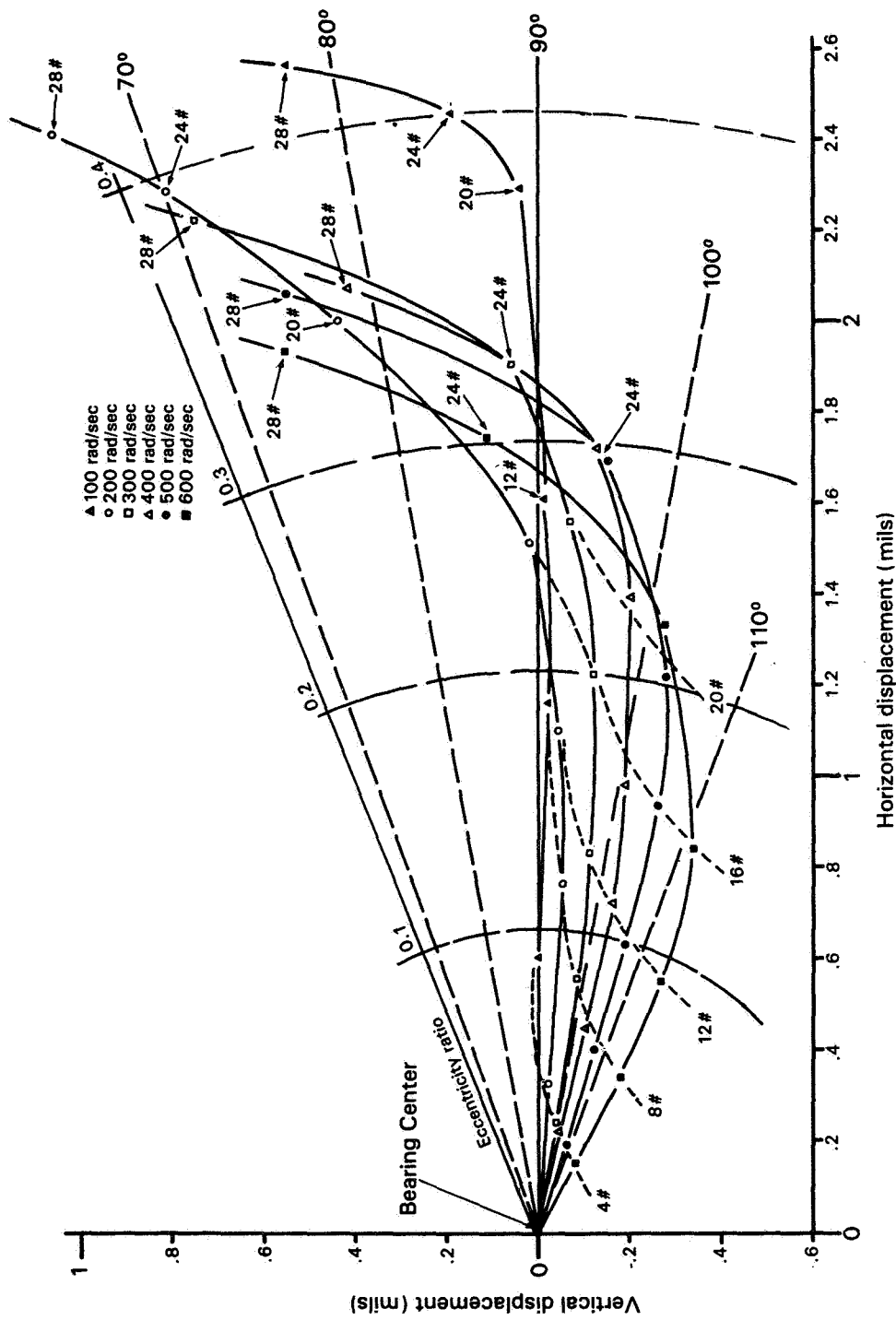
Vertical displacement (mils)

Bearing Center

Eccentricity ratio

▲ 100 rad/sec
○ 200 rad/sec
□ 300 rad/sec
△ 400 rad/sec
● 500 rad/sec
■ 600 rad/sec

90°
80°
70°
100°
110°

0.1
0.2
0.3
0.4

28#
24#
20#
16#
12#
8#
4#

Horizontal displacement (mils)

Figure 4. — Static deflection at rotative speeds of 100, 200, 300, 400, 500, and 600 rad/sec, oil outlet temperature of 98° F (35.6 cP), oil supply pressure of 5 psi, and static loads to 28 lb with clockwise rotation.
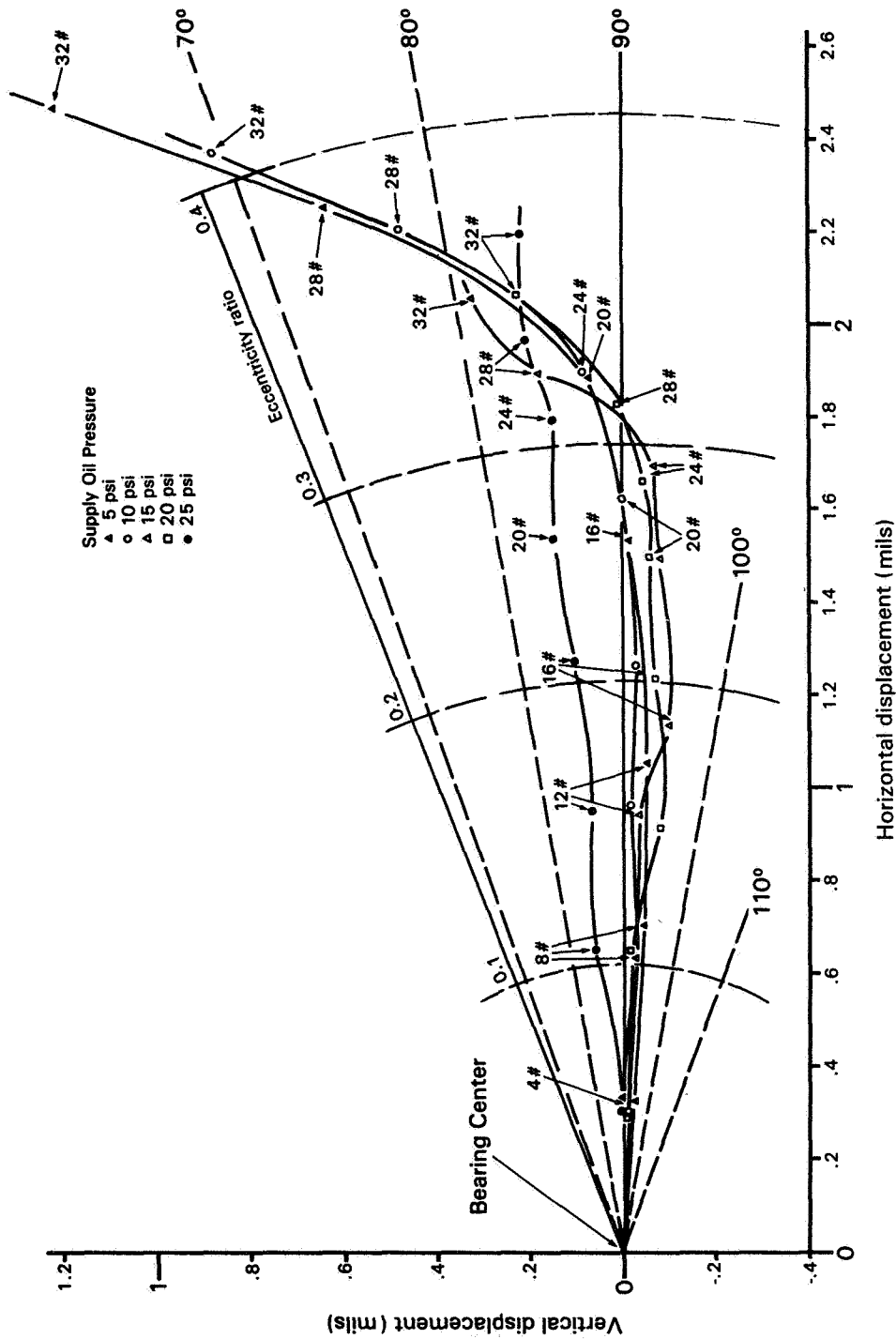
Figure 5. — Static deflection at oil supply pressures of 5, 10, 15, 20, and 25 psi, rotative speed of 200 rad/sec, oil outlet temperature of 90° F (35.6 cP), and static load to 32 lb with clockwise rotation.
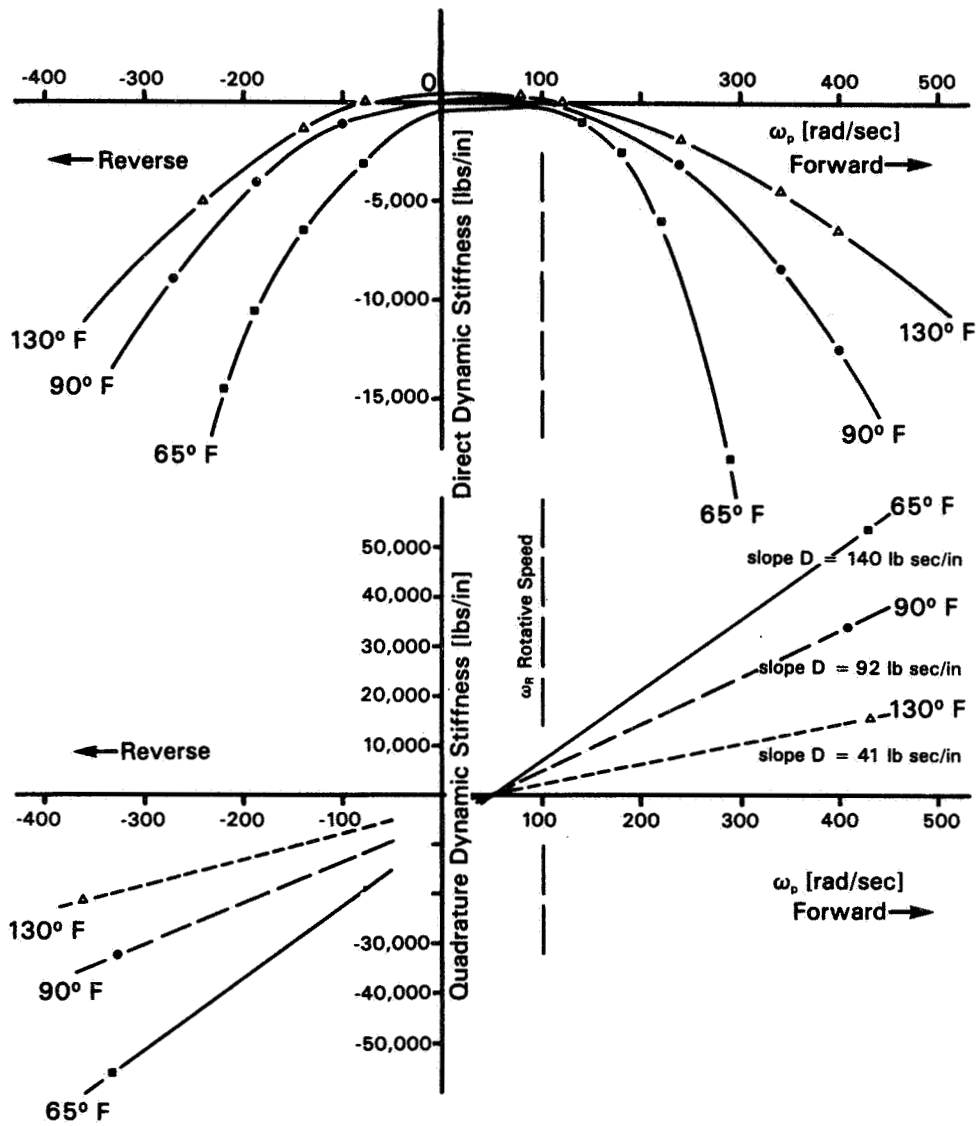
Figure 6. – Direct and quadrature dynamic stiffness at rotative speed of 100 rad/sec, oil outlet temperatures of 65°, 90°, and 130° F, oil supply pressure of 5 psi, and no static load.
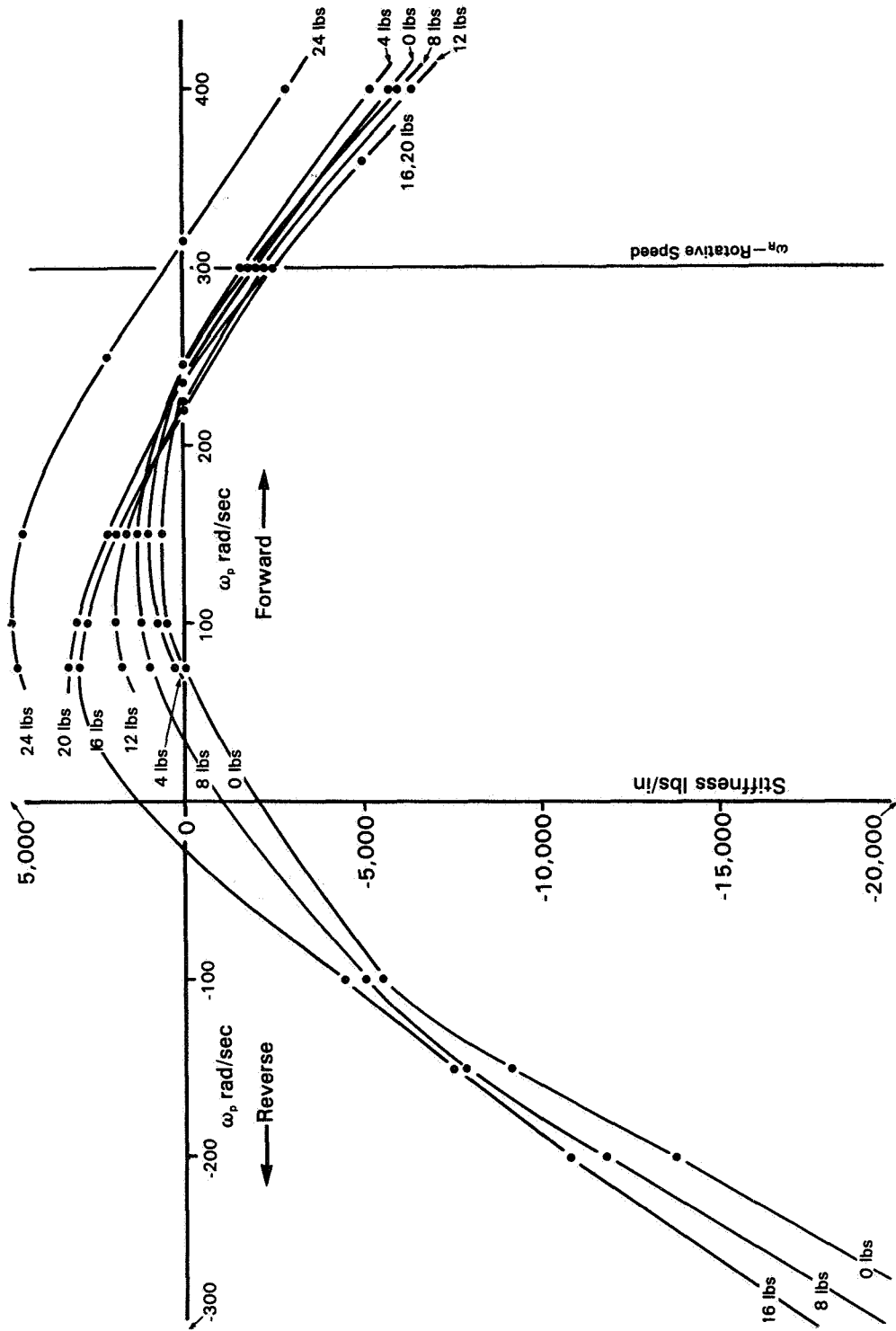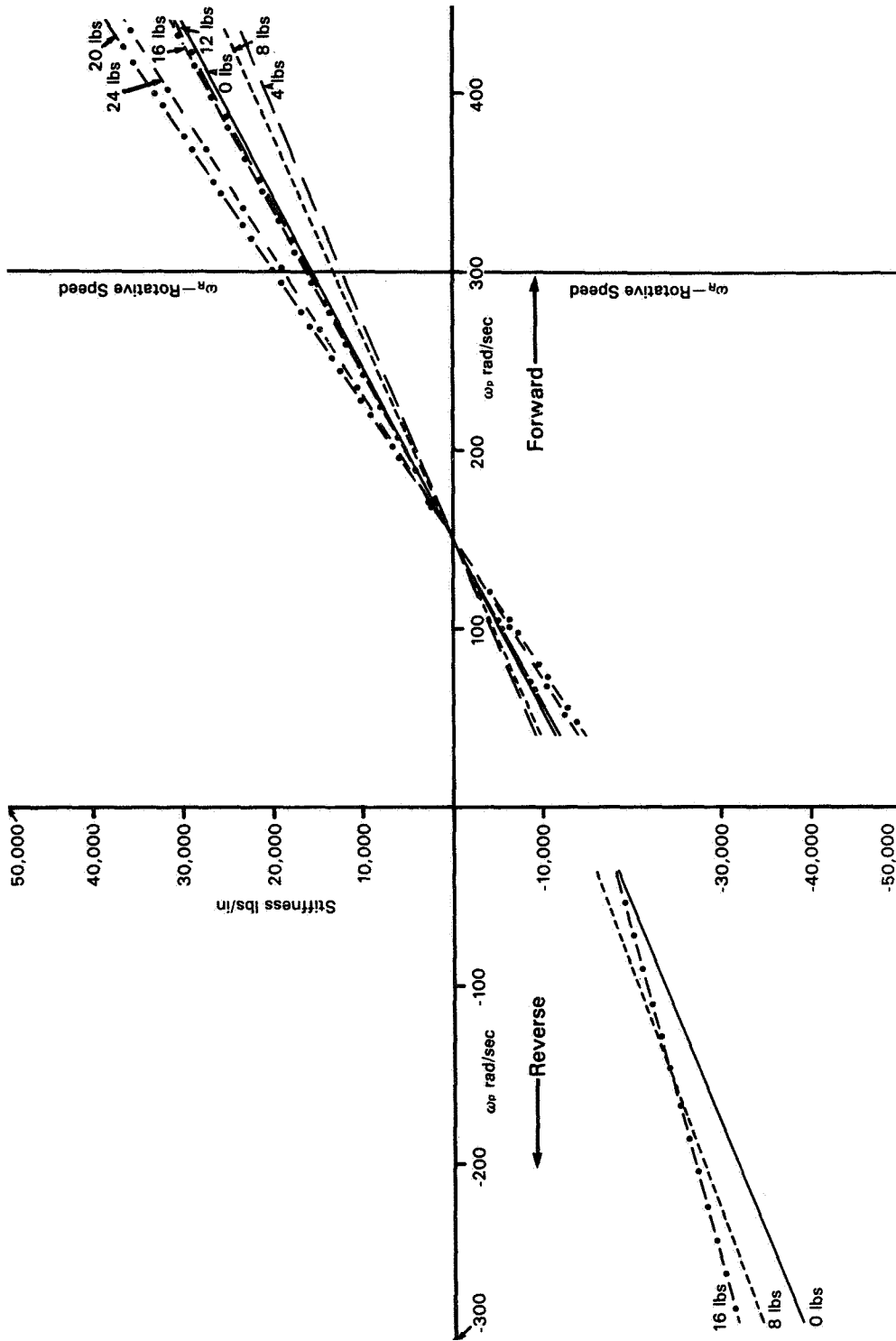
497

Figure 7. — Vertical direct dynamic stiffness at oil outlet temperature of 65° F (64.3 cP), rotative speed of 300 rad/sec, oil supply pressure of 5 psi, and static loads to 24 lb at P.

Figure 8. - Vertical quadrature dynamic stiffness at rotative speed of 300 rad/sec, oil outlet temperature of 65° F, oil supply pressure of 5 psi, and static loads to 24 lb.
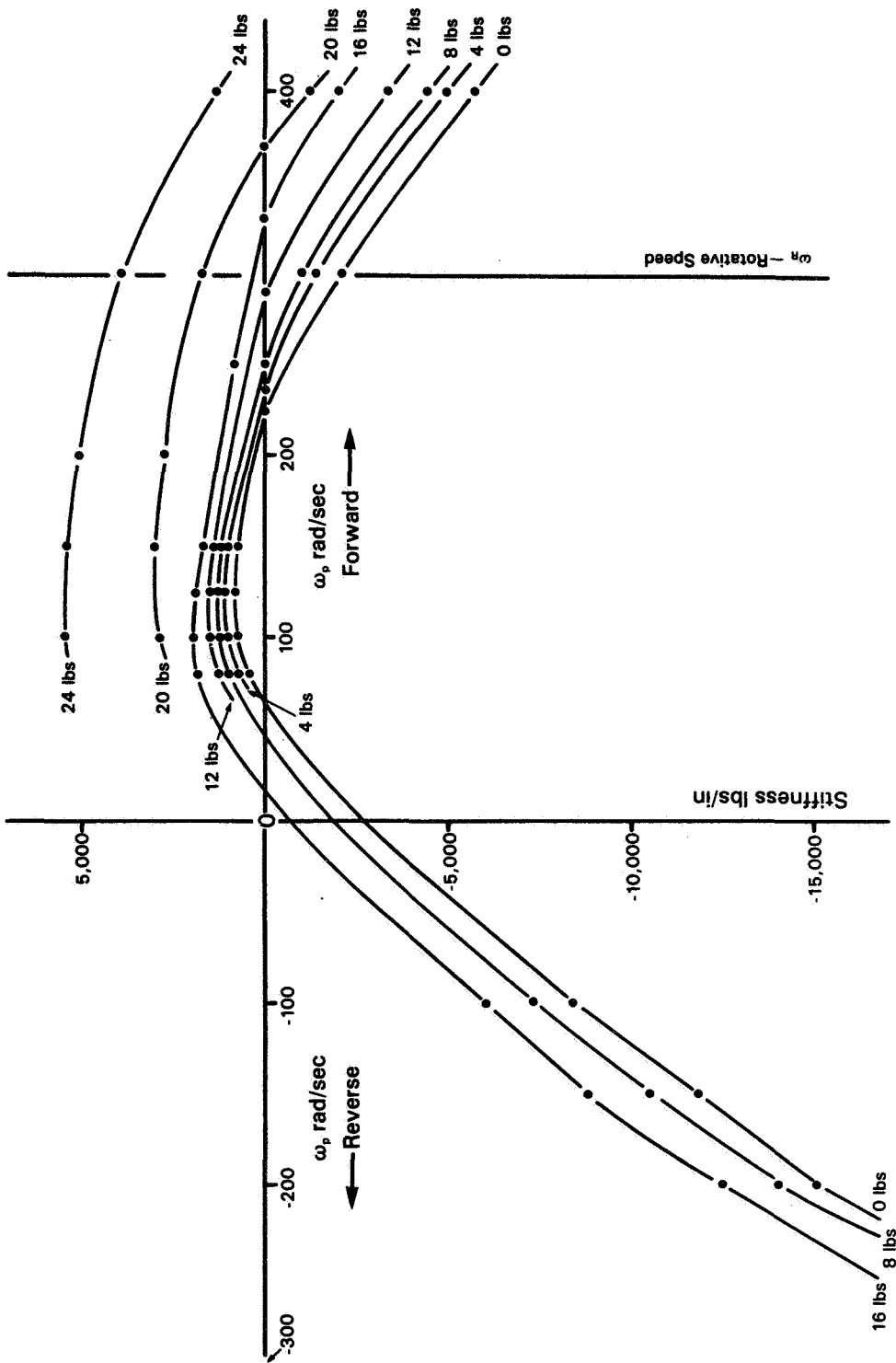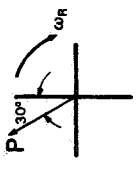
499

Figure 9. – Horizontal direct dynamic stiffness at oil outlet temperature of
65° F (64.3 cP), rotative speed of 300 rad/sec, oil supply pressure of 5 psi,
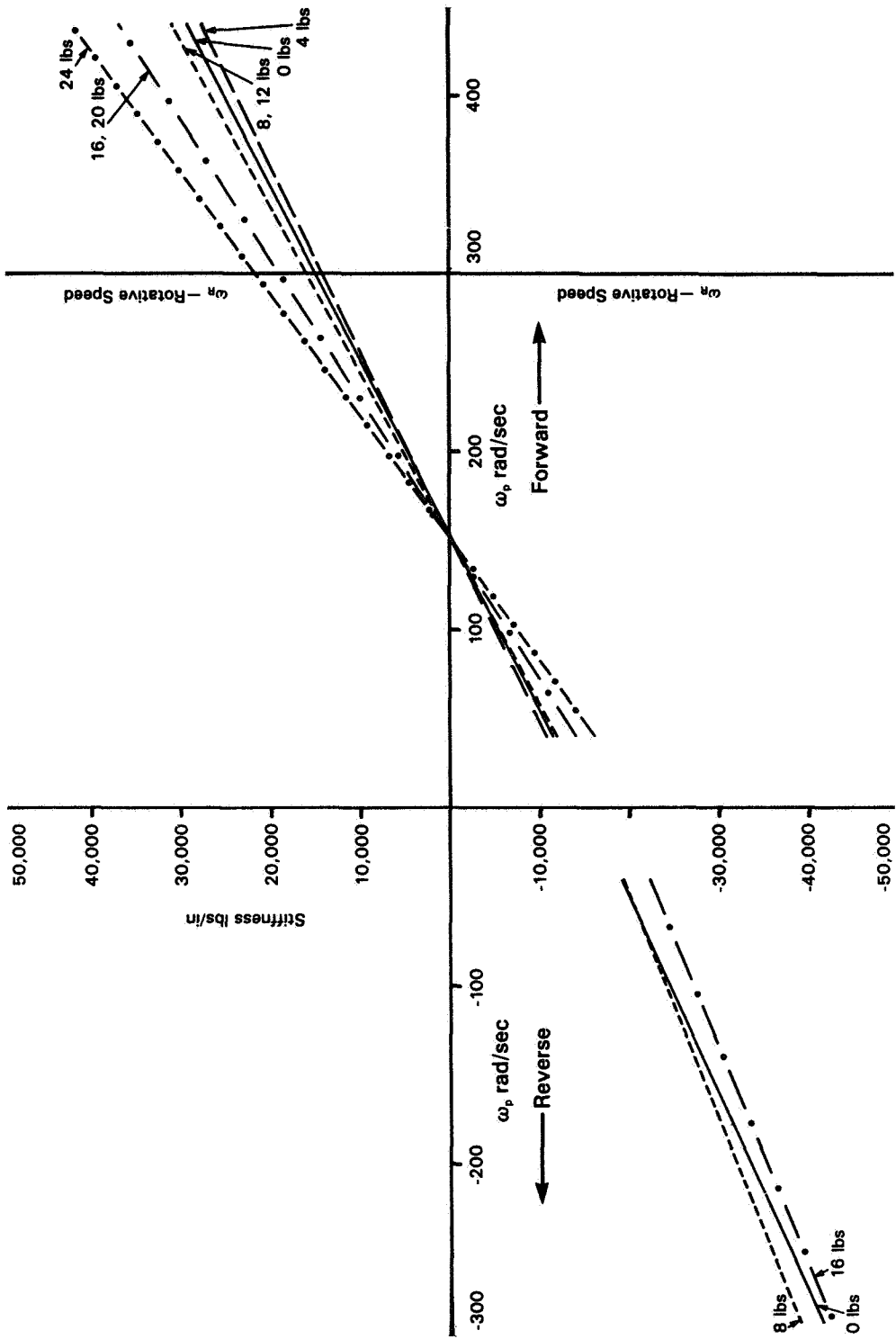and static loads to 24 lb at P.

500

Figure 10. - Horizontal quadrature dynamic stiffness at rotative speed of 300 rad/sec, oil outlet temperature of 65° F, oil supply pressure of 5 psi, and static loads of 0, 4, 8, 12, 16, 20, and 24 lb.

501